Untangling the complex origin of turbidite activity on the Calabrian Arc (Ionian Sea) over the last 60ka

Eléonore Köng, Sébastien Zaragosi, Jean-Luc Schneider, Thierry Garlan, Patrick Bachèlery, Laurine San Pedro, Chloé Seibert, Calypso Racine

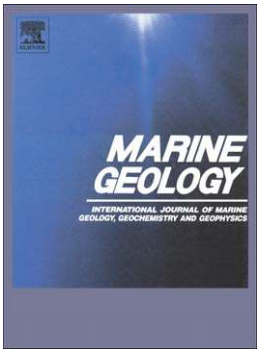

Untangling the complex origin of turbidite activity on the calabrian arc (Ionian sea) over the last 60 ka

Eléonore Köng, Sébastien Zaragosi, Jean-Luc Schneider, Thierry Garlan, Patrick Bachèlery, Laurine San Pedro, Chloé Seibert, Calypso Racine

PII: S0025-3227(15)30082-7
DOI: doi: 10.1016/j.margeo.2015.12.010
Reference: MARGO 5395

To appear in: *Marine Geology*

Received date: 26 August 2015
Revised date: 7 December 2015
Accepted date: 20 December 2015

Please cite this article as: Köng, Eléonore, Zaragosi, Sébastien, Schneider, Jean-Luc, Garlan, Thierry, Bachèlery, Patrick, Pedro, Laurine San, Seibert, Chloé, Racine, Calypso, Untangling the complex origin of turbidite activity on the calabrian arc (Ionian sea) over the last 60 ka, *Marine Geology* (2015), doi: 10.1016/j.margeo.2015.12.010

Untangling the complex origin of turbidite activity on the Calabrian Arc (Ionian Sea) over the last 60 ka

Authors

Eléonore Köng*[a], Sébastien Zaragosi[a], Jean-Luc Schneider[a], Thierry Garlan[b], Patrick Bachèlery[c], Laurine San Pedro[d], Chloé Seibert[a], Calypso Racine[a]

**corresponding author:* eleonore.kong@u-bordeaux.fr

[a] EPOC, UMR CNRS 5805, Université de Bordeaux, allée Geoffroy Saint-Hilaire, CS 50023, F-33615 Pessac cedex, France

[b] SHOM/DOPS/HOM/Sédimentologie, 13 rue du Chatellier, CS 92803, F-29228 Brest cedex 2, France

[c] LMV/OPGC, Université Blaise Pascal de Clermont-Ferrand, 5 rue Kessler, F-63038 Clermont-Ferrand, France

[d] Laboratoire Domaines Océaniques, UMR 6538, Université de Bretagne occidentale, IUEM, rue Dumont d'Urville, F-29280 Plouzané, France

Abstract

The Ionian Sea, due to the presence of two accretionary prisms, the Calabrian Arc and the Mediterranean Ridge, associated with the subduction of the Nubia plate and the Eurasia plate, is the witness of large and catastrophic turbidite events. These events are associated with high magnitude earthquakes and tsunamis. They lead an important gravity-driven sedimentary deposit in the Ionian basin. In this study, we analysed turbidite deposits in order to establish a calendar of the paleoseismicity and volcaniclastic events from Etna on the Calabrian Arc. Two gravity cores collected in a slope basin on the Calabrian Arc and in the Ionian abyssal plain record more than two hundred turbidites over the last 60,000 years. These turbidites were dated with a multi-proxy approach: radiometric dating, tephrochronology and sapropels.

The origin of the turbidites was studied with a sedimentary approach: grain-size, lithology, thin section, geochemistry of volcanic glass. The results suggest that three triggers are responsible for the deposits of turbidites. There are siliciclastic turbidites triggered by earthquakes and tsunamis waves, and volcaniclastic turbidites triggered by the Etna volcano eruptions or flank collapses. Co-seismic turbidites present different recurrence times depending on the location of the core. On the Calabrian Arc, recurrence times vary between 450 and 1,000 years according to the periods in time. On the abyssal plain, recurrence times are shorter and more regular: around every 240 years.

Keywords

Ionian Sea; accretionary prism; paleoearthquakes; paleotsunamis; co-seismic turbidites; volcaniclastic turbidites; natural hazard

1. Introduction

In active convergent margins, sediments related to earthquake activity are an important part of the sedimentation in submarine sedimentary successions. They provide the means to reconstruct the recurrence of paleo-earthquakes (Adams, 1990; Bernhardt et al., 2015; Goldfinger, 2011; Goldfinger et al., 2007; Gutiérrez-Pastor et al., 2013; Huh et al., 2004; Pouderoux et al., 2014, 2012). To reach such an objective, specific matter must be used: synchronicity of deposits over long distances in various topographically independent areas and arguments for contemporaneity with historic earthquakes.

The study of Kastens (1984) in the Calabrian Arc, indicates that it is a good place to conduct studies in paleoseismology. She emphasised three important necessary conditions to analyze the regional paleoseismicity: (1) to identify specific and distinctive earthquake-related sedimentary structures, (2) to date these specific structures, (3) to prove that the local conditions of sedimentation remain unchanged over a long period of time.

In the Ionian Sea, several basins record turbidite sedimentation. The Calabrian Arc, located in the southeast of Italy, displays a series of slope basins developed between accretionary ridges, and more distally, the Ionian abyssal plain. The presence of tephra and sapropels intercalated between turbidite enables ^{14}C radiocarbon age dating to be consolidated. Few studies have been devoted to this area (Kastens, 1984; Kastens and Cita, 1981; Polonia et al., 2015, 2013b). The most recent by Polonia et al. (2015, 2013b) focused on historical records (the last centuries) of co-seismic turbidites.

The present study aims to establish a record of past extreme sedimentary events in the Calabrian Arc over the last 60,000 years. We try to differentiate the various depositional processes, and to identify the origin of the turbidites. To achieve these goals, a multiproxy approach was applied to two sediment cores that were taken during the MOCOSED2012 oceanographic campaign, aboard RV *Pourquoi Pas ?*

2. Background

2.1. Geological background

The Ionian Sea comprises three main structures: the Calabrian accretionary prism from along the Sicilian and Calabrian coasts, the Ionian abyssal plain, as the relics of a subducting oceanic crust (de Voogd et al., 1992; Faccenna et al., 2004, 2001), and the Mediterranean ridge, an accretionary prism seated along the Greek coast that extends in the Levantine basin. The two accretionary prisms are linked to the subduction of the Nubia plate underneath the Eurasia plate at the very slow rate of 2-5mm/year (Fig. 1; D'Agostino et al., 2008; Devoti et al., 2008). The subduction is accompanied by the formation of the Tyrrhenian and the Aegean back-arc basins, active volcanic arcs in the Aeolian and Aegean Islands, and some isolated volcanoes such as Etna developed on the eastern Sicilian coast. Currently, Etna is a stratovolcano but its morphology has changed since it emerged 320,000 years ago. It started

as a subaerial fissure-type, evolved to a shield volcano around 220,000 years ago, then to a polygenic central-volcano around 120,000 years ago, and to the present day stratovolcano around 26,000 years ago (Kieffer, 1985).

Due to this tectonic configuration the Ionian Sea is an active seismic zone. Shallow earthquakes (depth < 100 km) located offshore or close to the coast (< 40 km inland) are associated with tsunamis. Earthquakes with magnitudes between 5.5 and 6.5 generate local tsunamis while earthquakes with magnitude greater than 6.5 generate regional or basin-wide tsunamis (Tinti et al., 2012).

The Calabrian Arc spreads over 65,000 km² with a slope lower than 1° to the south and is bordered by three structural units: the Malta Escarpment in the SW, the Apulia Escarpment in the NE and the Mediterranean ridge in the East (Fig. 1). The slow subduction, which is still locally active, drives an uplift in the Sicilian and Calabrian coasts during the Quaternary, estimated at about a 1mm/year by several authors (Catalano and De Guidi, 2003; Cucci, 2004). The Calabrian Arc is composed of two lobes, the Eastern Lobe (EL) bounded by the inner deformation front, and the Western Lobe (WL) bounded by the outer deformation front (Fig.1). Four main morphostructural domains were identified by (2011), segmented along strike with different deformations, uplift rates, structural style and basal detachment depth. From the NW to the SE, they distinguished (Fig. 1):

(1) The inner plateau is a flat area located between the continental slope and the pre-Messinian wedge at a water depth between 1300 to 1600 m. It is affected by 50 km wavelength undulations.

(2) The pre-Messinian wedge developed between 1600 and 3000 m deep. It is characterised by 10 km wavelength undulations with 250-300 m amplitudes.

(3) The slope terrace is a flat area between the pre and post-Messinian wedge with well-developed basins between accretionary ridges. These basins are 25 to 100 km wide and 50 m deep.

(4) The post-Messinian wedge is the most recent part of the Calabrian Arc. The basal detachment is located along the base of the Messinian evaporites salt bearing complex. It is characterised by 2.5 to 5 km wave length undulations with 100 m amplitudes.

2.2. Sedimentary transfers

In Sicily, three main rivers flow into the Ionian Sea: the Fiume Simeto, the Fiume Dittàino and the Fiume Alcàntara. Their lengths are respectively 113 km, 100 km and 52 km. They drain a total watershed of 5000 km² mainly composed of volcanic (Etna) and sedimentary rocks (Fig. 1). In the southeast of Sicily, small rivers less than 50 km long drain a watershed inferior to 500 km², which are exclusively composed of carbonate rocks (Fig. 1). In the south of the Calabrian province, river lengths are smaller than 25 km in contrast to the northern part where rivers flowing to the Taranto valley are more developed (Coste, 2014). They drain metamorphic and sedimentary rocks (Fig. 1).

The Calabrian Arc shows a complex morphology that constrains sediment gravity flows (Fig.1; modified from Polonia et al., (2013b). Offshore Calabria and Sicily, canyons and channels incise the entire continental shelf from 0 to 2000 m in water depth (Coste, 2014). These canyons and channels transport the sediments from the shelf to the basin. Along the Malta escarpment, canyons also incise the continental shelf from 100 to 3000 m in water depth. As shown on the eastern slope of the Gela Basin (Minisini et al., 2007), the canyons deeply incised the shelf above the last sea level lowstand, activating sediment transport from the Malta shelf.

Below 2000 m in water depth on the Calabrian Arc, channeling is unclear. Gravity flows are more diffuse, constrained by the geometry of accretionary ridges and slope basins. On the western side of the Western lobe, a drainage axis between the Malta shelf and the Calabrian Arc probably drains the sediment flux from Sicily to the Ionian abyssal plain, preventing sediments from reaching the Calabrian Arc (fig. 1).

Turbidite activity on the Calabrian Arc is usually linked to earthquakes and associated with tsunamis (Cita and Aloisi, 1999; Kastens, 1984; Kastens and Cita, 1981; Polonia et al., 2013a, 2013b). Studies covering the last 1,000 years linked turbidite sedimentation to last centuries' major earthquakes (Polonia et al., 2013b).

3. Methods

3.1. Sediment core analysis

Bathymetry and sub-bottom seismic lines: high-resolution multibeam bathymetry data and sub-bottom seismic lines were collected during the SHOM (French Hydrographic and Oceanographic Marine Service) oceanographic campaign MOCOSED2012 on RV *Pourquoi Pas ?* The multibeam echosounder Reson^{TM} 7150 (12 kHz) with a spatial resolution of 40 m, and the sub-bottom sediment profiler ECHOES 3500 (between 1.8 and 5.3 kHz) were used.

Piston cores analysed in this study were collected during the oceanographic campaign MOCOSED2012 with a 4 ton Calypso corer. Table 1 summarises core collection information. The cores were analysed through a multiproxy approach, which comprise the following.

X-ray imagery: thin slabs (15 mm thick) were sampled and analysed with the SCOPIX X-ray image processing tool (Migeon et al., 1998). X-rays allow the distinction between various densities with grey levels in order to highlight sedimentary structures.

Grain size: The cores were sampled with a path varying from 1 to 50 mm, depending on changes in sedimentological structures. Sediment was analysed with a Laser Diffraction

Malvern™ Granulometer MASTER SIZER S (UMR EPOC). The 1st mode of the grain-size distribution was calculated with GRADISTAT v8 (Blott and Pye, 2001). Total grain size distribution is presented with grain size on x-axis and depth on y-axis, the colour scale shows relative abundance of each grain-size fraction in percentage (from dark blue for low abundance to dark red color for high abundance). Grain size highlights coarser sedimentary structures and allows to link layers with a depositional mechanism like turbidites for example.

Magnetic susceptibility (MS) was acquired by using a Bartington™ MS2E1 pointer sensor with 10 mm resolution. Data acquisition was performed with a sampling interval of 10 mm. It is used to highlight volcaniclastic layers when MS values are high and sapropels when MS values are very low.

Geochemical data were acquired on a cm-scale with an AVAATECH™ XRF core-scanner (UMR EPOC) using the 10 and 30 kV instrumental settings. An element ratio was used to avoid influence of sediment porosity and water content. Ti and Al were used as denominators because of their stability in sediments (lithogenic nature, resistance to chemical weathering, concentration in major sources; Calvert et al., 2001). Ca/Ti ratio was used as a proxy to estimate the relative oceanic or terrestrial influences (Cuven et al., 2013; Goudeau et al., 2014), high values representing the oceanic source and low values representing the terrestrial source. S+Br/Al highlight the sapropel layers when the value is high because of the affinity of S and Br with organic matter (Warning and Brumsack, 2000; Ziegler et al., 2008).

Petrographic observations were performed with a Leica™ DM6000 B Digital Microscope on thin sections of remarkable sequences. Thin sections were obtained on fresh cores after induration with a resin (Zaragosi et al., 2006). They allow the high-resolution observation of preserved sedimentary structures.

3.2. Stratigraphy

Radiometric dating was performed at the "Laboratoire de Mesure du Carbone 14" in Saclay (SacA) through the "ARTEMIS" radiocarbon age dating program. Analyses were performed on planktonic foraminifera collected in the pelagic facies, *Globigerinoides ruber* when enough material was available, bulk when there was not. Results are summarised in table 2.

Tephrochronology: Volcanic glasses were collected in tephra deposits and analysed with a CAMECA SX100 electron microprobe at the University of Clermont-Ferrand (CNRS UMR LMV). Geochemistry of major oxides, SiO_2 and alkaline sum (Na_2O, K_2O), allow the classification of volcanic glasses thanks to (Le Bas et al., 1986) lava classification.

Age model: ^{14}C radiometric dates are calibrated by MARINE13 curve (Reimer et al., 2013). The present day Mediterranean reservoir age is higher than 500 years (Siani et al., 2000) but cores record 60 ka of sedimentation. Without any constraint on the reservoir age changes over the last 60 ka, a global ocean reservoir of 400 years (Reimer et al., 2013) was chosen. Age models were performed by an R software package Clam 2.2 (Blaauw, (2010) with a linear interpolation method and 1 cm resolution. The age model for the upper part of the core has been exclusively based on ^{14}C dates. Tephra layers and one sapropel layer are present in the upper part of the core. These peculiar layers were not used for the age model because of the variability of their ages provided in the literature. However, for the lower part of the core (age > 30 ka), the age model is constrained by the composition and resulting ages of the tephra layers.

4. Results

4.1. Core location setting

Core KC14 (Table 1), 1566 cm long, was collected in a 15 km² well stratified slope basin (Fig. 2a,b) in the Western lobe of the post-Messinian wedge, in the slope terrace zone (Fig. 1). This slope basin is oblong and enclosed by two N45° accretionary ridges of respectively 40 to

80 m high and 10 to 30 m high from the base of the basin. On the seismic profile, 20 to 30 m thick deposits appear stratified.

Core KC01 (Table 1), 1045 cm long, was collected on the western edge of the Ionian abyssal plain between the Ionian abyssal plain and the Malta Escarpment (Fig. 2c,d). This zone is located downstream from the western drainage axis (Fig. 1). Figure 2d displays well-stratified parallel deposits up to 60 m thick, forming relief around 10 m high.

4.2. Lithofacies

Five lithofacies were identified in all cores, on the basis of grain size, XRF data measurements, thin-section analysis and lithological composition.

Hemipelagic (Hp; Fig. 3: in white): hemipelagic intervals consist of blue/green to brown, fine-grained (3 < 1st Mode < 4 µm), clay layers with planktonic foraminifera fossils. Hp layers are characterised by high Ca/Ti ratio (between 20 and 30).

Siliciclastic turbidite (TS; Fig. 3: in black; e.g. Fig. 8): the deposits present a sharp, mainly erosive, base. They form massive layers and range in grain size from coarse silt to fine sand (30 < 1st Mode < 100 µm). Eventually, the deposits change into a homogeneous clay sequence at the top (4 < 1st Mode < 5 µm). The layers display planar laminations and rippled intervals. The sediment fraction > 125 µm is mainly composed of biotite and muscovite, with minor quartz, woody debris, rare planktonic and benthic foraminifera, and pteropod shell fragments. It is geochemically characterised by a low Ca/Ti ratio (around 10) in most cases, and has a magnetic susceptibility comprised between 50 and 200 SI. These deposits correspond to turbidites with a siliciclastic signature. The Ca/Ti ratio is higher (between 9 and 15) for a turbidite between 25 and 67 cm in depth in core KC14. It is very high (between 17 and 26) in three particular layers even though the lithological composition appears similar: a one meter thick turbidite between 497 and 397 cm in depth in core KC14 and two successive turbidites between 272 and 221 cm in depth in core KC01 (Fig. 3; in dark grey).

Volcaniclastic turbidite (TV) (Fig. 3: in red; e.g. Fig. 9): the deposits display sharp to erosive bases. They range from a very fine sand layer, which is generally massive, with an occasional light reverse grading (30 < 1st Mode < 100 µm) that vertically changes to a very fine normally-graded interval (4 < 1st Mode < 5 µm). This sequence shows planar laminations and is composed of scoria, alkali feldspars, pyroxenes, and rare benthic foraminifera. It is characterised by a high magnetic susceptibility over 100 SI in most cases. These layers were interpreted as a volcaniclastic turbidite sequence as described by (Schneider et al., 2001)). Scoriaceous particles from three of these turbidites (Fig.3: red stars) were analysed. Results are summarised in figure 5b and table 5. They have a trachyte to trachy-andesite composition.

Tephra (Fig. 3: in green): tephra layers present a progressive base and top, and are composed of volcanic glasses with minerals (pyroxene, amphibole, alkali feldspar).

Sapropel (Fig. 3: in light green; Fig. 4): the grain size of this layer is coarser than for hemipelagic facies: 6 < 1st Mode < 8 µm. It is rich in organic marine matter, foraminifera and pteropods.

4.3. Stratigraphy

KC14

Seven *radiometric dates* were performed in the upper part of KC14 (Fig. 3: white stars; Table 2). Ages range from 3,284 ± 74 years cal BP to 31,278 ± 276 years cal BP.

Sapropel layer S1 is observed in KC14 between 87 and 175 cm in depth (Fig. 3). Its age is comprised between 10,213 ± 88 and 3,284 ± 74 years cal BP (Fig. 3). A thin section in a part of this sapropel is presented on figure 4. The important thickness, 88 cm, is explained by the presence of thin turbidite layers which split the sapropel into 8 main parts as shown by X-ray radiography data and thin section's observation (Fig. 4). The sapropel layers mainly contain planktonic foraminifera and pteropod shells.

Six *tephra layers* were recovered in KC14 (Fig. 3: green stars). Their geochemical compositions are summarised in table 3, dates obtained with the age model in table 4. Geochemical analyses suggest three different signatures.

- Tephra 1 is located at 140 cm in depth in the core within the sapropel S1 layer (Fig. 4). It is 0.5 cm thick and displays a rhyolitic composition. It is dated, from the age model, at 9.0 ± 0.1 ka.
- Tephra 2 is located at 314 cm in depth in the core (Fig. 4). It is 1.5 cm thick and has a trachytic composition. It is dated, from the age model, at 16.7 ± 0.2 ka.
- Tephra 3 is located at 363 cm in depth in the core (Fig. 4). It is 0.3 cm thick and has a trachytic composition. It is dated, from the age model, at 18.8 ± 0.3 ka.
- Tephra 4 is located at 609 cm in depth in the core (Fig. 4). It is 0.3 cm thick and has a rhyolitic composition. It is dated, from the age model, at 29.8 ± 0.4 ka.
- Tephra 5 is located at 865 cm in depth in the core (Fig. 4). It is 1.5 cm thick and has a phonolitic composition. It can't be dated from the age model, because it is located below the ^{14}C dated interval.
- Tephra 6 is located at 1258 cm in depth in the core (Fig. 4). It is a volcaniclastic turbidite of 31 cm thick and has a phonolitic composition. Like tephra 5, it can't be dated.

KC01

Seven *radiometric dates* were obtained for KC01 (Fig. 3: white stars; Table 2) for the upper one-third of the core, from 12,676 ± 67 years cal BP to 29,100 ± 393 years cal BP.

Two *tephra layers* were found in KC01 (Fig. 3: green stars). Their geochemical compositions are summarised in table 3. Dates obtained from the age model are given in table 4.

- The first is 0.2 cm thick and is located 20 cm in depth in the core (Fig. 4). Its composition can't be analysed because the pyroclasts are too fine. This tephra is dated, from the age model, at 9.9 ± 1.1 ka.
- The second is 0.3 cm thick and is located 174 cm deep in the core (Fig.4). It displays a trachytic composition. It is dated, from the age model, at 18.8 ± 0.3 ka.

5. Discussion

5.1. Tephra versus ^{14}C age model

In core KC14, some tephra layers can be identified by comparing their compositions with published data (Fig. 5, Table 3):

- Tephra 1 (9.0 ± 0.1 ka) has the same composition as the E1 Lipari eruption. E1 was dated in literature at 7,700 yrs BP (Fontugne et al., 1989; Paterne et al., 1988; Siani et al., 2004). The age obtained in this study is 1300 yrs older. The deposit of this rhyolitic tephra layer is coeval with the Lipari's IX eruptive cycle. It should correspond to the inland fall and surge deposits Gabellotto-Fiume Bianco that occurred between 11.4 ka and 8.6 ka (Bigazzi and Bonadonna, 1973; Gioncada et al., 2003).
- Tephra 2 (16.7 ± 0.2 ka) can be correlated to the Y1 from Etna dated at 16.8 ka (Albert et al., 2013; Insinga et al., 2014; Keller et al., 1978).
- Tephra 3 (18.8 ± 0.3 ka) can be correlated to the pre-Y1 from Etna dated at 18.1 ka (Albert et al., 2013; Insinga et al., 2014; Keller et al., 1978).
- Tephra 4 (29.8 ± 0.4 ka) can be linked to the Aeolian Islands because of its high content in SiO_2 (> 70%). This layer has no reference in literature.
- Tephra 5 geochemistry corresponds to Y5 from Phlegrean Fields dated at 38 ka (Di Girolamo and Keller, 1972; Insinga et al., 2014; Keller et al., 1978; Murat, 1984;

Narcisi, 1996; Narcisi and Vezzoli, 1999; Ninkovich and Heezen, 1967; Rosi and Sbrana, 1987; Vezzoli, 1991; Vinci, 1985; Wulf et al., 2004).

- Tephra 6 is a primary volcaniclastic turbidite with a Phlegrean Fields signature, probably the Y7 dated at 55 ka (Insinga et al., 2014; Keller et al., 1978; Wulf et al., 2004).

In core KC01, only the second tephra layer was identified. Its geochemical signature is very similar to the pre-Y1 layer in KC14 (Fig. 5(Albert et al., 2013; Keller et al., 1978; Paterne et al., 1988; Siani et al., 2004; Vezzoli, 1991; Wulf et al., 2008, 2004).

The age models presented previously (Fig. 6 and 7), including radiometric dates (until 30 ka) and tephra data (for the period older than 30 ka), is supported between 30 ka and the Present by the dating of the first three upper tephra layers and sapropel S1. Indeed, dates obtained from the age model are close to the dates found in literature (Table 4). Turbidites have not been removed for the calculation of the age model because their thickness is relatively constant. Removing turbidite layers and construct an age model solely with hemipelagic intervals is very difficult. It suggests that we have to perfectly distinguish hemipelagic intervals from turbidites and to take erosion due to turbidites deposition into account. Sediment rates presented in figures 6 and 7 were calculated with two methods: between the ^{14}C radiocarbon dating and from the age model with a 5000 yrs step. They show very similar variations and values (e.g. Toucanne et al., 2008). Eventually, for the long core, the construction of an age model including turbidite deposits of regular thickness generates fewer errors than an age model built with a hemipelagic interval extracted between turbidites.

5.2. Correlation between the cores

Cores KC14 and KC01 record the same time interval, according to the age model, from the Holocene to 60-70 ka. The absence of sapropel number 3 (S3), dated at 83 ka (S3 basis)

by (Emeis et al., 2004) confirms the lower limits. The sedimentation rates of the two cores are similar, between 10 and 30 cm/ka. However, turbidite layers in KC14 are pluri-decimeters thick, whereas in KC01 they are centimeters thick. This contrast in thickness and the difference of the number of layers in each core do not facilitate their correlation, except for one event with a different geochemical signature (high Ca/Ti ratio), the thickest siliciclastic turbidites with an age estimated around 21 ka (Fig. and 10).

5.3. Recurrence times

KC14 is 1566 cm long and records around 70 turbidites, whereas KC01 is 1045 cm long and records around 250 turbidites. Recurrence times were calculated for siliciclastic and volcaniclastic turbidites with a 10 ka time window, based on dates obtained with the age models (Fig. 6 and 7). Each interval time (10 ka) was divided by the number of turbidite layers to obtain an average return time of turbidites (Fig. 11). The 10 ka time window was chosen depending on the maximum interval between two ^{14}C radiometric dates.

Siliciclastic turbidites

Recurrence time presented in figure 11 highlights two different time-scales for siliciclastic turbidites (TS).

- The first is comprised between 230 and 250 years. It represents the turbidite recurrence time in KC01 core.
- The second is comprised between 450 and 1,000 years. It represents the turbidite recurrence time in KC14 core.

Volcaniclastic turbidites

Recurrence time for volcaniclastic turbidites was determined for KC14 core where they are exclusively present. It is comprised between 1,000 and 3,000 years. The most active period with a return time around 700-800 years is identified between 19 and 14 ka.

5.4. Turbidite activity on an accretionary prism

Compared to its counterparts, the Makran or Hikurangi prism, the Calabrian accretionary prism presents lower tectonic activity. It covers a large distance of around 200-300 km from the Italian coast to the abyssal plain with a slope inferior to 1° (Polonia et al., 2011; Praeg et al., 2009). Convergence rates are around 2-5 mm/year (D'Agostino et al., 2008; Devoti et al., 2008).

For comparison, the Makran accretionary prism for instance, shows convergence rates ten times higher, comprised between 2 and 4 cm/year (Ellouz-Zimmermann et al., 2007), a width of 100-150 km and a slope angle comprised between 1° and 2° (Kukowski et al., 2001). Turbidite activity in the Makran accretionary prism varies depending on fluvial influx and tectonic activity (Bourget et al., 2011, 2010). Sediment rates are high during the Holocene, from 233 cm/ka in the abyssal plain to 129.8 cm/ka in the canyons. However, return times are only around 250 years in the Oman abyssal pain.

On the Hikurangi trough (New Zealand), Pouderoux et al. (2014) studied submarine paleoseismology based on a 16 ka turbidite record. This accretionary prism presents a high convergence rate of 5 cm/year, has a width of 150 km and a steep slope of around 4° (Beavan et al., 2002; DeMets et al., 1994). This important activity leads to a high sediment rate from 15 to 110 cm/ka. The return time for co-seismic turbidites is 230 years (Pouderoux et al., 2012).

On the Calabrian Arc, incision of the prism occurs only in its upper part. Channelisation disappears below 2000 m in water depth. This can be explained by the relatively flat morphology of the Calabrian Arc, combined with underdeveloped fluvial systems (<100 km in length). Compared to the Hikurangi and Makran prisms, sedimentation rates comprised

between 10 and 30 cm/ka, are low. However, turbidite return times in the abyssal plain (around 240 years) is similar.

Sediment rates are very different, from 10 to 233 cm/ka. This variability can be explained by the different convergence rates and the climatic background of the geographic area: depending on the intensity of the tectonic activity and the presence, or absence, of important fluviatile systems. However, it appears that the seismic cycle recorded by turbidite deposits (around 240 yrs) is the same on the three prisms previously presented.

5.5. Various origins of the turbidite activity over the last 60 ka

The various sedimentary facies previously described, siliciclastic and volcaniclastic turbidites, suggest several processes and origins for sediments.

Earthquakes

The steady gravity-driven sedimentation over the last 60 ka on the Calabrian Arc shows that the influence of glacio-eustatism and floods on sedimentation was probably limited. Only volcaniclastic turbidites disturb co-seismic siliciclastic turbidite sedimentation. Earthquakes seem to be the main triggering process used to explain turbidite events on the Calabrian Arc (Kastens, 1984; Polonia et al., 2013b).

The siliciclastic turbidites studied here are those which are more likely to be linked to earthquakes, allowing us to propose a calendar of these events for the last 60 ka. Our data indicates that the average earthquake return time is ~240 years for the 30-10 ka interval from the abyssal plain sedimentary record, based on the record of 250 turbidites. The record on the prism provides a return time comprised between 450 and 1,000 years, based on the record of 75 turbidites.

Recurrence times determined in the present study are lower than those previously published: between 1000 and 3000 yrs by Kastens (1984), 500 yrs by Polonia et al.(2013b), and between 100 and 700 yrs by Polonia et al. (2015). However, they remain with the same range of pluri-centennial time intervals. This study allows us to constrain the hypotheses proposed by Polonia et al. (2013b). These authors suggest that only the largest events are recorded on the accretionary prism when in fact all events are recorded in the Ionian abyssal plain. Return times are twice as long in slope basins on the Calabrian Arc (between 450 and 1,000 years) than in the abyssal plain (240 years). To explain the shorter return time in the abyssal plain, we suggest that the drainage axis in the west probably drains Sicilian and Malta shelf sediments directly to the abyssal plain, leading to a more important turbidite activity.

The sediment in core KC01 derives from a large drainage area, which includes both the subaerial and the submarine slopes of the Sicily and Malta escarpment. Submarine sediment reworking may be triggered by earthquake activity and may lead to the emplacement of co-seismic turbidites (Fig. 12). However, it is very difficult to make the distinction between the various possible origins of these turbidites. The recurrence times estimated for the turbidites in core KC01, by their constancy over the last 60 ka, strongly suggest a dominant co-seismic control of the gravity-driven sedimentation.

The estimation of earthquake return times for the Calabrian Arc is difficult. It depends on the available sedimentary records, and is also influenced by the activity of numerous seismogenic faults in the area (Galli et al., 2008). As suggested by our study, earthquake return time reconstructions are also disturbed by a multiplicity of processes highlighted over long period of time.

Tsunamis

Often related to earthquakes, tsunamis are a triggering mechanism mentioned in literature. (Kastens and Cita, 1981), and then (Cita and Aloisi, 1999), worked on a megaturbidite, called Augias, deposited in the Ionian abyssal plain after the passage of a tsunami wave. They linked the tsunami wave with the Minoan Santorini caldera collapse, in the Bronze Age, at 3.6 ka. Then, Polonia et al. (2013a) linked a megaturbidite with a tsunamigenic earthquake that occured AD 365 in Crete.

Two siliciclastic deposits dated in cores around 3.2 and 21 ka show higher Ca/Ti ratios than the other turbidites, especially for the one at 21 ka recorded both in the Calabrian Arc and the Ionian abyssal plain.

The first one (3.2 ka) could be contemporaneous with the Augias megaturbidite described in the Ionian abyssal plain. On the Calabrian Arc, the deposit is thin (50 cm). It probably results from the destabilisation of sediments on the Calabrian Arc during the passage of a tsunami wave. Two events could be the triggers of this tsunami wave: the Minoan Santorini caldera collapse or the AD 365 Cretan earthquakes. Recent studies suggest that the tsunami wave triggered by the Santorini collapse did not reach the Ionian Sea (Pareschi et al., 2006), and in fact linked the Augias megaturbidite to the AD 365 Cretan earthquake (Polonia et al., 2013a). The absence of ^{14}C radiocarbon dating on the top of the deposit doesn't allow us to provide a definitive answer.

The 21 ka deposit could be linked to a caldera formation, called Cape-Riva, that occured in Santorini around 21 ka (Dominey-Howes and Minos-Minopoulos, 2004) or an earthquake on the Greek or the Italian coast.

Volcanism

Core KC14 also contains volcaniclastic turbidites. Some of these turbidites were analysed; their trachytic to trachy-andesitic composition merge with the chemical

characteristics of the Etna volcanism, at least for the major elements (Fig.5b and Table 5; (Peccerillo, 2005).

The number of volcaniclastic turbidites is higher, between 19 and 14 ka, with a return time lower than 1,000 years. This period is coeval to a succession of collaspses of the eastern Etna flank in the Ionian Sea during the emplacement of the present-day stratovolcano (Calvari et al., 2004, 1998; Guest et al., 1983). Scars of some of these collapses can still be recognised nowadays in the volcano's morphology. They formed a depression called Valle del Bove.

Two other high activity periods are recognized but not linked with specific events. The first occurs around 30 ka and the second around 60 ka. Both show return times between 1,000 and 2,000 years.

No volcaniclastic turbidites were recorded in the abyssal plain (KC01). Turbidites were either washed off along the slope of the prism by following events, or were never deposited in this area (Fig. 12). This could be explained by the fact that volcaniclastic turbidites could have less energy than co-seismic turbidites because of their lower volume and, possibly, because of the high density of some volcaniclastic particles within the clastic fraction.

6. Conclusion

This study presents the first paleoseismic record over the last 60 ka in the Calabrian Arc, but also suggests a large variability of the origin of sediments and depositional processes. Sedimentary record is comprised of siliciclastic and volcaniclastic turbidites, hemipelagic clay, sapropels and tephra layers. Three different processes for turbidite deposition, characterised by different return times, are recognised:

- Earthquakes: co-seismic deposits represent the main part of the sedimentary record. Return times are centennial to millennial in scale, between 450 and 1,000 years on the

Calabrian Arc during the last 60 ka, and around 240 years in the Ionian abyssal plain between 30 and 10 ka.

- Tsunami: the record of a probable tsunami has been found in the abyssal plain and in a slope basin on the Calabrian Arc: the Augias turbidite and a tsunami dated around 21 ka.
- Volcanoes: Etna flank collapses or eruptive phases seem to be recorded in the Calabrian Arc. The most active period has been identified between 19 and 14 ka. During this period, corresponding to the Valle del Bove formation, the events return time is at a millennial scale.

The slope basins on the Calabrian Arc record less turbidites than the Ionian abyssal plain. In effect, on the Calabrian Arc turbidites are unchannelised below 2000 m in depth, whereas the Ionian abyssal plain drains sediment from both the Sicilian coast and the Malta shelf thanks to the drainage axis along the Calabrian Arc (Fig. 12).

Acknowledgements

We thank the SHOM (hydrological and oceanographic marine service) for the data, DGA (French Defence Procurement Agency, French Ministry of Defense) and CNRS (National Center of Scientific Research) of Normandy for PhD thesis funding, the 'ARTEMIS' technical platform for radiocarbon age dating. We are also grateful to EPOC technicians and engineers: P. Lebleu, I. Billy, B. Martin, O. Ther, B. Cosson, L. Rossignol and M.-H. Castera for the data acquisition. We thank J.-L. Devidal for his assistance with the electron microprobe. We finally acknowledge Lucia Hudson-Turner who provides English-language support.

References

Adams, J., 1990. Paleoseismicity of the Cascadia subduction zone: Evidence from turbidites off the Oregon-Washington margin. Tectonics 9, 569–583.

Albert, P.G., Tomlinson, E.L., Lane, C.S., Wulf, S., Smith, V.C., Coltelli, M., Keller, J., Lo Castro, D., Manning, C.J., Müller, W., Menzies, M.A., 2013. Late glacial explosive activity on Mount Etna: Implications for proximal–distal tephra correlations and the synchronisation of Mediterranean archives. J. Volcanol. Geotherm. Res. 265, 9–26. doi:10.1016/j.jvolgeores.2013.07.010

Beavan, J., Tregoning, P., Bevis, M., Kato, T., Meertens, C., 2002. Motion and rigidity of the Pacific Plate and implications for plate boundary deformation. J. Geophys. Res. Solid Earth 1978–2012 107, ETG–19.

Bernhardt, A., Melnick, D., Hebbeln, D., Lückge, A., Strecker, M.R., 2015. Turbidite paleoseismology along the active continental margin of Chile – Feasible or not? Quat. Sci. Rev. 120, 71–92. doi:10.1016/j.quascirev.2015.04.001

Bigazzi, G., Bonadonna, F.P., 1973. Fission Track Dating of the Obsidian of Lipari Island (Italy). Nature 242, 322–323. doi:10.1038/242322a0

Blaauw, M., 2010. Methods and code for "classical" age-modelling of radiocarbon sequences. Quat. Geochronol. 5, 512–518. doi:10.1016/j.quageo.2010.01.002

Blott, S.J., Pye, K., 2001. GRADISTAT: a grain size distribution and statistics package for the analysis of unconsolidated sediments. Earth Surf. Process. Landf. 26, 1237–1248.

Bourget, J., Zaragosi, S., ELLOUZ-ZIMMERMANN, N., Mouchot, N., Garlan, T., SCHNEIDER, J., Lanfumey, V., Lallemant, S., 2011. Turbidite system architecture and sedimentary processes along topographically complex slopes: the Makran convergent margin. Sedimentology 58, 376–406.

Bourget, J., Zaragosi, S., Ellouz-Zimmermann, S., Ducassou, E., Prins, M., Garlan, T., Lanfumey, V., Schneider, J.-L., Rouillard, P., Giraudeau, J., 2010. Highstand vs. lowstand turbidite system growth in the Makran active margin: Imprints of high-frequency external controls on sediment delivery mechanisms to deep water systems. Mar. Geol. 274, 187–208.

Calvari, S., Tanner, L.H., Groppelli, G., 1998. Debris-avalanche deposits of the Milo Lahar sequence and the opening of the Valle del Bove on Etna volcano (Italy). J. Volcanol. Geotherm. Res. 87, 193–209.

Calvari, S., Tanner, L.H., Groppelli, G., Norini, G., 2004. Valle del Bove, eastern flank of Etna volcano: a comprehensive model for the opening of the depression and implications for future hazards. Geophys. Monogr. Ser. 143, 65–75.

Calvert, S.., Pedersen, T.., Karlin, R.., 2001. Geochemical and isotopic evidence for post-glacial palaeoceanographic changes in Saanich Inlet, British Columbia. Mar. Geol. 174, 287–305. doi:10.1016/S0025-3227(00)00156-0

Catalano, S., De Guidi, G., 2003. Late Quaternary uplift of northeastern Sicily: relation with the active normal faulting deformation. J. Geodyn. 36, 445–467. doi:10.1016/S0264-3707(02)00035-2

Cita, M.B., Aloisi, G., 1999. Deep-sea tsunami deposits triggered by the explosion of Santorini (3500 y BP), eastern Mediterranean. Sediment. Geol. 135, 181–203. doi:10.1016/S0037-0738(00)00071-3

Coste, M., 2014. Les processus sédimentaires, depuis la pente continentale jusqu'au bassin, en contexte de tectonique active: analyse comparée entre la Marge Calabro-Ionienne et la Marge Ligure durant les derniers 5 Ma. Dr. Diss.

Cucci, L., 2004. Raised marine terraces in the Northern Calabrian Arc (Southern Italy): a~ 600 kyr-long geological record of regional uplift. Ann. Geophys. 47.

Cuven, S., Paris, R., Falvard, S., Miot-Noirault, E., Benbakkar, M., Schneider, J.-L., Billy, I., 2013. High-resolution analysis of a tsunami deposit: Case-study from the 1755 Lisbon tsunami in southwestern Spain. Mar. Geol. 337, 98–111. doi:10.1016/j.margeo.2013.02.002

D'Agostino, N., Avallone, A., Cheloni, D., D'anastasio, E., Mantenuto, S., Selvaggi, G., 2008. Active tectonics of the Adriatic region from GPS and earthquake slip vectors. J. Geophys. Res. Solid Earth 1978–2012 113.

DeMets, C., Gordon, R.G., Argus, D.F., Stein, S., 1994. Effect of recent revisions to the geomagnetic reversal time scale on estimates of current plate motions. Geophys. Res. Lett. 21, 2191–2194.

de Voogd, B., Truffert, C., Chamot-Rooke, N., Huchon, P., Lallemant, S., Le Pichon, X., 1992. Two-ship deep seismic soundings in the basins of the Eastern Mediterranean Sea (Pasiphae cruise). Geophys. J. Int. 109, 536–552.

Devoti, R., Riguzzi, F., Cuffaro, M., Doglioni, C., 2008. New GPS constraints on the kinematics of the Apennines subduction. Earth Planet. Sci. Lett. 273, 163–174.

Di Girolamo, P., Keller, J., 1972. Zur stellung des Grauen Campanischen Tuffs innerharlb des quartären Vulkanismus Campaniens (Süditalien).«. Ber Naturforsch Ges Freibg. IBr 61, 85–92.

Dominey-Howes, D., Minos-Minopoulos, D., 2004. Perceptions of hazard and risk on Santorini. J. Volcanol. Geotherm. Res. 137, 285–310. doi:10.1016/j.jvolgeores.2004.06.002

Ellouz-Zimmermann, N., Lallemant, S., Castilla, R., Mouchot, N., Leturmy, P., Battani, A., Buret, C., Cherel, L., Desaubliaux, G., Deville, E., 2007. Offshore frontal part of the Makran Accretionary prism: The Chamak survey (Pakistan), in: Thrust Belts and Foreland Basins. Springer, pp. 351–366.

Emeis, K.-C., Sakamoto, T., Wehausen, R., Brumsack, H.-J., 2004. The sapropel record of the eastern Mediterranean Sea — results of Ocean Drilling Program Leg 160. Palaeogeogr. Palaeoclimatol. Palaeoecol. 158, 371–395. doi:10.1016/S0031-0182(00)00059-6

Faccenna, C., Becker, T.W., Lucente, F.P., Jolivet, L., Rossetti, F., 2001. History of subduction and back arc extension in the Central Mediterranean. Geophys. J. Int. 145, 809–820.

Faccenna, C., Piromallo, C., Crespo-Blanc, A., Jolivet, L., Rossetti, F., 2004. Lateral slab deformation and the origin of the western Mediterranean arcs. Tectonics 23.

Fontugne, M.R., Paterne, M., Calvert, S.E., Murat, A., Guichard, F., Arnold, M., 1989. Adriatic deep water formation during the Holocene: implication for the reoxygenation of the deep Eastern Mediterranean sea. Paleoceanography 4, 199–206.

Galli, P., Galadini, F., Pantosti, D., 2008. Twenty years of paleoseismology in Italy. Earth-Sci. Rev. 88, 89–117. doi:10.1016/j.earscirev.2008.01.001

Gioncada, A., Mazzuoli, R., Bisson, M., Pareschi, M.., 2003. Petrology of volcanic products younger than 42 ka on the Lipari–Vulcano complex (Aeolian Islands, Italy): an example of volcanism controlled by tectonics. J. Volcanol. Geotherm. Res. 122, 191–220. doi:10.1016/S0377-0273(02)00502-4

Goldfinger, C., 2011. Submarine paleoseismology based on turbidite records. Annu. Rev. Mar. Sci. 3, 35–66.

Goldfinger, C., Morey, A.E., Nelson, C.H., Gutiérrez-Pastor, J., Johnson, J.E., Karabanov, E., Chaytor, J., Eriksson, A., 2007. Rupture lengths and temporal history of significant earthquakes on the offshore and north coast segments of the Northern San Andreas Fault based on turbidite stratigraphy. Earth Planet. Sci. Lett. 254, 9–27. doi:10.1016/j.epsl.2006.11.017

Goudeau, M.-L.S., Grauel, A.-L., Tessarolo, C., Leider, A., Chen, L., Bernasconi, S.M., Versteegh, G.J.M., Zonneveld, K.A.F., Boer, W., Alonso-Hernandez, C.M., De Lange, G.J., 2014. The Glacial–Interglacial transition and Holocene environmental changes in sediments from the Gulf of Taranto, central Mediterranean. Mar. Geol. 348, 88–102. doi:10.1016/j.margeo.2013.12.003

Guest, J.E., Chester, D.K., Duncan, A.M., 1983. The valle del bove, Mount Etna: Its origin and relation to the stratigraphy and structure of the volcano. J. Volcanol. Geotherm. Res. 21, 1–23. doi:10.1016/0377-0273(84)90013-1

Gutiérrez-Pastor, J., Nelson, C.H., Goldfinger, C., Escutia, C., 2013. Sedimentology of seismo-turbidites off the Cascadia and northern California active tectonic continental margins, northwest Pacific Ocean. Mar. Geol. 336, 99–119.

Huh, C., Su, C., Liang, W., Ling, C., 2004. Linkages between turbidites in the southern Okinawa Trough and submarine earthquakes. Geophys. Res. Lett. 31.

Insinga, D.D., Tamburrino, S., Lirer, F., Vezzoli, L., Barra, M., De Lange, G.J., Tiepolo, M., Vallefuoco, M., Mazzola, S., Sprovieri, M., 2014. Tephrochronology of the astronomically-tuned KC01B deep-sea core, Ionian Sea: insights into the explosive activity of the Central Mediterranean area during the last 200 ka. Quat. Sci. Rev. 85, 63–84. doi:10.1016/j.quascirev.2013.11.019

Kastens, K.A., 1984. Earthquakes as a triggering mechanism for debris flows and turbidites on the Calabrian Ridge. Mar. Geol. 55, 13–33. doi:10.1016/0025-3227(84)90130-0

Kastens, K.A., Cita, M.B., 1981. Tsunami-induced sediment transport in the abyssal Mediterranean Sea. Geol. Soc. Am. Bull. 92, 845–857.

Keller, J., Ryan, W., Ninkovich, D., Altherr, R., 1978. Explosive volcanic activity in the Mediterranean over the past 200,000 yr as recorded in deep-sea sediments. Geol. Soc. Am. Bull. 89, 591–604.

Kieffer, G., 1985. Evolution structurale et dynamique d'un grand volcan polygénique: stades d'édification et activité actuelle de l'Etna(Sicile). Dr. Diss.

Kukowski, N., Schillhorn, T., Huhn, K., von Rad, U., Husen, S., Flueh, E.R., 2001. Morphotectonics and mechanics of the central Makran accretionary wedge off Pakistan. Mar. Geol. 173, 1–19.

Le Bas, M., Le Maitre, R., Streckeisen, A., Zanettin, B., 1986. A chemical classification of volcanic rocks based on the total alkali-silica diagram. J. Petrol. 27, 745–750.

Migeon, S., Weber, O., Faugeres, J.-C., Saint-Paul, J., 1998. SCOPIX: a new X-ray imaging system for core analysis. Geo-Mar. Lett. 18, 251–255.

Minisini, D., Trincardi, F., Asioli, A., Canu, M., Foglini, F., 2007. Morphologic variability of exposed mass-transport deposits on the eastern slope of Gela Basin (Sicily channel). Basin Res. 19, 217–240.

Murat, A., 1984. Séquences et paléoenvironnements marins quaternaires: Une marge active: L'arc hellénique oriental. Dr. Diss.

Narcisi, B., 1996. Tephrochronology of a late quaternary lacustrine record from the Monticchio maar (Vulture volcano, Southern Italy). Quat. Sci. Rev. 15, 155–165. doi:10.1016/0277-3791(95)00045-3

Narcisi, B., Vezzoli, L., 1999. Quaternary stratigraphy of distal tephra layers in the Mediterranean—an overview. Glob. Planet. Change 21, 31–50.

Ninkovich, D., Heezen, B., 1967. Physical and chemical properties of volcanic glass shards from Pozzuolana ash, Thera Island, and from upper and lower ash layers in Eastern Mediterranean deep sea sediments.

Pareschi, M.T., Favalli, M., Boschi, E., 2006. Impact of the Minoan tsunami of Santorini: Simulated scenarios in the eastern Mediterranean. Geophys. Res. Lett. 33.

Paterne, M., Guichard, F., Labeyrie, J., 1988. Explosive activity of the South Italian volcanoes during the past 80,000 years as determined by marine tephrochronology. J. Volcanol. Geotherm. Res. 34, 153–172. doi:10.1016/0377-0273(88)90030-3

Peccerillo, A., 2005. Plio-quaternary volcanism in Italy. Springer.

Polonia, A., Bonatti, E., Camerlenghi, A., Lucchi, R.G., Panieri, G., Gasperini, L., 2013a. Mediterranean megaturbidite triggered by the AD 365 Crete earthquake and tsunami. Sci Rep 3.

Polonia, A., Panieri, G., Gasperini, L., Gasparotto, G., Bellucci, L.G., Torelli, L., 2013b. Turbidite paleoseismology in the Calabrian Arc subduction complex (Ionian Sea). Geochem. Geophys. Geosystems.

Polonia, A., Romano, S., Çağatay, M.N., Capotondi, L., Gasparotto, G., Gasperini, L., Panieri, G., Torelli, L., 2015. Are repetitive slumpings during sapropel S1 related to paleo-earthquakes? Mar. Geol. 361, 41–52. doi:10.1016/j.margeo.2015.01.001

Polonia, A., Torelli, L., Mussoni, P., Gasperini, L., Artoni, A., Klaeschen, D., 2011. The Calabrian Arc subduction complex in the Ionian Sea: Regional architecture, active deformation, and seismic hazard. Tectonics 30, TC5018. doi:10.1029/2010TC002821

Pouderoux, H., Lamarche, G., Proust, J.-N., 2012. Building an 18 000-year-long paleo-earthquake record from detailed deep-sea turbidite characterisation in Poverty Bay, New Zealand. Nat Hazards Earth Syst Sci 12, 2077–2101.

Pouderoux, H., Proust, J.-N., Lamarche, G., 2014. Submarine paleoseismology of the northern Hikurangi subduction margin of New Zealand as deduced from Turbidite record since 16 ka. Quat. Sci. Rev. 84, 116–131. doi:10.1016/j.quascirev.2013.11.015

Praeg, D., Ceramicola, S., Barbieri, R., Unnithan, V., Wardell, N., 2009. Tectonically-driven mud volcanism since the late Pliocene on the Calabrian accretionary prism, central Mediterranean Sea. Mar. Pet. Geol. 26, 1849–1865. doi:10.1016/j.marpetgeo.2009.03.008

Reimer, P.J., Bard, E., Bayliss, A., Beck, J.W., Blackwell, P.G., Bronk Ramsey, C., Buck, C.E., Cheng, H., Edwards, R.L., Friedrich, M., 2013. IntCal13 and Marine13 radiocarbon age calibration curves 0-50,000 years cal BP.

Rosi, M., Sbrana, A., 1987. Phlegrean fields. Consiglio nazionale delle ricerche.

Schneider, J.-L., Le Ruyet, A., Chanier, F., Buret, C., Ferrière, J., Proust, J.-N., Rosseel, J.-B., 2001. Primary or secondary distal volcaniclastic turbidites: how to make the distinction? An example from the Miocene of New Zealand (Mahia Peninsula, North Island). Sediment. Geol. 145, 1–22.

Siani, G., Paterne, M., Arnold, M., Bard, E., Métivier, B., Tisnerat, N., Bassinot, F., 2000. Radiocarbon reservoir ages in the Mediterranean Sea and Black Sea. Radiocarbon 42, 271–280.

Siani, G., Sulpizio, R., Paterne, M., Sbrana, A., 2004. Tephrostratigraphy study for the last 18,000 14C years in a deep-sea sediment sequence for the South Adriatic. Quat. Sci. Rev. 23, 2485–2500. doi:10.1016/j.quascirev.2004.06.004

Tinti, S., Graziani, L., Brizuela, B., Maramai, A., Gallazzi, S., 2012. Applicability of the Decision Matrix of North Eastern Atlantic, Mediterranean and connected seas Tsunami Warning System to the Italian tsunamis. Nat. Hazards Earth Syst. Sci. 12, 843–857. doi:10.5194/nhess-12-843-2012

Toucanne, S., Zaragosi, S., Bourillet, J.F., Naughton, F., Cremer, M., Eynaud, F., Dennielou, B., 2008. Activity of the turbidite levees of the Celtic–Armorican margin (Bay of Biscay) during the last 30,000 years: Imprints of the last European deglaciation and Heinrich events. Mar. Geol. 247, 84–103. doi:10.1016/j.margeo.2007.08.006

Vezzoli, L., 1991. Tephra layers in Bannock basin (eastern Mediterranean). Mar. Geol. 100, 21–34.

Vinci, A., 1985. Distribution and chemical composition of tephra layers from eastern Mediterranean abyssal sediments. Mar. Geol. 64, 143–155.

Viti, M., Mantovani, E., Babbucci, D., Tamburelli, C., 2011. Plate kinematics and geodynamics in the Central Mediterranean. Act. Tecton. Circum-Adriat. Reg. 51, 190–204. doi:10.1016/j.jog.2010.02.006

Warning, B., Brumsack, H.-J., 2000. Trace metal signatures of eastern Mediterranean sapropels. Palaeogeogr. Palaeoclimatol. Palaeoecol. 158, 293–309.

Wulf, S., Kraml, M., Brauer, A., Keller, J., Negendank, J.F.W., 2004. Tephrochronology of the 100 ka lacustrine sediment record of Lago Grande di Monticchio (southern Italy). Quat. Int. 122, 7–30. doi:10.1016/j.quaint.2004.01.028

Wulf, S., Kraml, M., Keller, J., 2008. Towards a detailed distal tephrostratigraphy in the Central Mediterranean: The last 20,000 yrs record of Lago Grande di Monticchio. J. Volcanol. Geotherm. Res. 177, 118–132. doi:10.1016/j.jvolgeores.2007.10.009

Zaragosi, S., Bourillet, J.-F., Eynaud, F., Toucanne, S., Denhard, B., Van Toer, A., Lanfumey, V., 2006. The impact of the last European deglaciation on the deep-sea turbidite systems of the Celtic-Armorican margin (Bay of Biscay). Geo-Mar. Lett. 26, 317–329. doi:10.1007/s00367-006-0048-9

Ziegler, M., Jilbert, T., de Lange, G.J., Lourens, L.J., Reichart, G., 2008. Bromine counts from XRF scanning as an estimate of the marine organic carbon content of sediment cores. Geochem. Geophys. Geosystems.

Fig. 1: Location map and physiography of the Calabrian Arc. Bathymetry is issued from GEBCO (http://www.gebco.net/) and contours are in meters. The Calabrian Arc structure of

the map and longitudinal depth profiles are derived from (Polonia et al., 2011). The accretionary ridge presents two lobes, western and eastern, segmented by two wedges, pre and post-messinian. Red crosses show sediment cores used in this study. Blue lines represent the location of the main rivers, canyons and channels (solid lines) and unchanneled streams (dashed lines; modified from Polonia et al., 2013b). The brown line represents the sea level lowstand for the last glaciation (-120m). Simplified geology of Italy derived from the Italian servizi litologica (http://sgi.isprambiente.it/geoportal/). The kinematic map of the Mediterranean Sea is modified from Viti et al. (2011).

Fig. 2: Close-up on the cores locations. (a) and (c) Bathymetry is issued from MOCOSED2012 cruise. Longitudinal depth profiles are at the same scale and present the local morphology. (b) and (d) CHIRP profiles from MOCOSED2012 cruise present stratigraphy of the core's locations areas, their locations are represented with a red line on (a) and (c).

Fig. 3: Stratigraphy, sedimentary logs and facies occurrence. Core's locations are presented on fig. 1. White stars indicate the calibrated AMS-14C dates (Table 2). Green stars indicate tephra. Red stars indicate analysed volcaniclastic turbidites with electron microprobe. Grain size distribution is represented by cartography of the relative abundance of each fraction in percentages (from dark blue for low abundance to dark red color for high abundance). Magnetic susceptibility of the sediments in SI, Ca/Ti and S+Br/Al ratios, turbidites number per meter of sediments. TS corresponds to siliciclastic turbidites, TV to volcaniclastic turbidites and Hp to hemipelagic sediment.

Fig. 4: Grain size measurements, X-ray pictures and thin section of sapropel S1 present in core KC14. Grain size distribution is presented by cartography of the relative abundance of each fraction in percentages (from dark blue for low abundance to dark red color for high abundance). PPL corresponds to plane polarised light and XPL to crossed polarised light. S1 is interbedded by a turbidite layer and a tephra linked to the Lipari volcano. Core location in fig. 1.

Fig. 5: (a) Total Alkali versus Silica (TAS – wt. %) diagram (Le Bas et al., 1986) classifies the glass shards as phonolitic, trachytic and rhyolitic populations in composition. (b) Total Alkali versus Silica (TAS – wt. %) diagram (Le Bas et al., 1986) classifies the pumices from volcaniclastic turbidites as trachytic populations in composition. H.A is the molecular ratio of the peralkaline index defined by H.A. = mol(Na_2O+K_2O)/Al_2O_3. These compositional characters are compatible with Campanian, Etnean and Aeolian provenance. Geochemical oxide's values in tables 3 and 5.

Fig. 6: Age model (black line) and its error margin (grey areas) of core KC14 were built using a linear interpolation implemented with the CLAM package v.2.2 of R software (Blaauw, 2010). Radiometric dates are in blue, tephra in green and sapropel S1 in light green. Y1, Y5 and Y7 correspond to tephra layers from the Phlegrean Fields. Sediment rates are calculated using two methods: between the ^{14}C radiocarbon dates and by a 5 ka interval from the age model. Core location in fig. 1.

Fig. 7: Age model (black line) and its error margin (grey areas) of core KC01 built using a linear interpolation implemented with the CLAM package v.2.2 of R software (Blaauw, 2010). Radiometric dates are in blue and tephra in green. Y1 corresponds to tephra layers

from the Phlegrean Fields. Sediment rates are calculated using two methods: between the ^{14}C radiocarbon dates and by a 5 ka interval from the age model. Core location in fig. 1.

Fig. 8: Grain size measurements, X-ray pictures and thin section of a siliciclastic turbidite (TS facies) present in core KC14. Grain size distribution is presented by cartography of the relative abundance of each fraction in percentages (from dark blue for low abundance to dark red color for high abundance). PPL corresponds to plane polarised light and XPL to crossed polarised light. Core location in fig. 1.

Fig. 9: Grain size measurements, X-ray pictures and thin section of a volcaniclastic turbidite (TV facies) and Y1 tephra present in core KC14. Grain size distribution is presented by cartography of the relative abundance of each fraction in percentage (from dark blue for low abundance to dark red color for high abundance). PPL correspond to plane polarized light and XPL to crossed polarized light. Core location in fig. 1.

Fig. 10: Sedimentary logs, calibrated radiometric dates (yrs BP; Table 2), tephra and correlation of the sedimentary cores.

Fig. 11: Return times of co-seismic turbidites calculated by a 10 ka interval. Cores locations in fig. 1.

Fig. 12: Reconstruction of the main underwater flow on the Calabrian Arc.

Table 1: Cores' locations in degrees, cores' length, corers' lengths and depths sampling.

Cores	Latitude	Longitude	Cores' Lenght (cm)	Corers' Lenght (cm)	Depth (m)

KC01	35.5540	17.0276	1045	1200	3950
KC14	36.5704	16.3297	1566	2400	3338

Table 2: Radiometric ages for samples collected in hemipelagic sediments.

Core	Core depth (cm)	Nature of sample	Radiocarbon age (BP)			Calibrated age (BP)		
KC01	67.3	Planktonic foram.: *G. ruber*	11,180	±	35	12,676	±	90
	101	Planktonic foram.	12,940	±	80	14,719	±	415
	176	Planktonic foram.: *G. ruber*	16,100	±	50	18,937	±	139
	215	Planktonic foram.	17,900	±	90	21,141	±	298
	278	Planktonic foram.: *G. ruber*	18,530	±	60	21,997	±	219
	329	Planktonic foram.	21,380	±	110	25,319	±	295
	393.5	Planktonic foram.	25,450	±	180	29,100	±	413
KC14	69	Planktonic foram.: *G. ruber*	3,415	±	20	3,284	±	74
	122	Planktonic foram.	7,495	±	40	7,949	±	97
	161	Planktonic foram.: *G. ruber*	9,370	±	40	10,213	±	88
	260	Planktonic foram.: *G. ruber*	12,675	±	40	14,216	±	204
	364	Planktonic foram.	16,040	±	60	18,881	±	137
	561	Planktonic foram.	23,380	±	160	27,292	±	322
	637	Planktonic foram.	27,820	±	200	31,278	±	276

Table 3: Electron microprobe analyses of glass shards in tephra layers.

Core	Core depth (cm)	SiO_2	TiO_2	Al_2O_3	FeO	MnO	MgO	CaO	Na_2O	K_2O	P_2O_5	Total
KC14	140	71.18	0.05	12.54	1.27	0.11	0.02	0.75	3.52	4.89	0.00	94.34
		71.66	0.05	12.72	1.47	0.06	0.00	0.78	3.75	4.89	0.10	95.48
	363	60.90	1.20	16.91	4.55	0.18	1.57	3.06	5.76	3.49	0.24	97.86
		60.54	1.16	16.85	4.13	0.40	1.49	3.29	5.68	3.37	0.37	97.27
	609	72.66	0.06	12.47	1.06	0.00	0.00	0.66	3.52	4.64	0.02	95.10
		73.47	0.06	12.17	1.16	0.20	0.00	0.63	3.10	4.63	0.00	95.41
		73.60	0.10	12.57	1.30	0.11	0.03	0.65	3.10	4.85	0.04	97.01
		73.47	0.08	12.42	1.42	0.07	0.01	0.64	3.79	4.92	0.02	96.84
	865	61.54	0.38	18.76	2.74	0.23	0.52	1.72	5.40	8.05	0.07	99.41
		61.39	0.35	18.82	2.60	0.19	0.34	1.72	6.69	7.11	0.07	99.28
	1258	61.30	0.57	18.54	2.87	0.25	0.28	1.02	7.77	6.24	0.01	98.84
		61.28	0.51	18.56	2.52	0.21	0.28	0.96	8.11	6.08	0.03	98.53
		61.00	0.53	18.22	2.74	0.39	0.29	1.07	8.22	6.08	0.03	98.57
KC01	174	60.22	1.15	16.73	4.42	0.16	1.39	3.11	5.83	3.48	0.27	96.76
		60.30	1.20	17.00	4.45	0.09	1.66	3.33	5.89	3.52	0.44	97.88
		59.88	1.40	16.62	4.60	0.24	1.38	3.27	5.48	3.49	0.34	96.69

Table 4: Dates of sapropel S1 and tephra obtained with the age model compared with literature.

Core	Sapropel	Tephra	Position (cm)	Thickness (cm)	Age (yrs)	Age in literature (yrs)	Reference
KC14	S1		87-175	88	top 4,865 ± 117		
					base 10,775 ± 162	9,500 ± 220	Emeis et al., 2004
		Gabellotto Fiume Bianco	140	0.5	8,992 ± 123	11.4 to 8.6	Bigazzi and Bonadonna, 1973; Gioncada et al., 2003
		Y1	314	1.5	16,635 239	16,763 ± 203	Insinga et al., 2014
		pre-Y1	363	0.3	18,838 ± 261	18,140 ± 160	Insinga et al., 2014
		Aeolian Islands	609	0.3	29,810 ± 391	unknown	
KC01	S1		abscent				
		Gabellotto Fiume Bianco	20	0.2	9,855 ± 1118	11.4 to 8.6	Bigazzi and Bonadonna, 1973; Gioncada et al., 2003
		pre-Y1	174	0.3	18,823 ± 253	18,140 ± 160	Insinga et al., 2014

Table 5: Electron microprobe analyses of pumices in volcaniclastic layers.

Core	Core depth (cm)	SiO_2	TiO_2	Al_2O_3	FeO	MnO	MgO	CaO	Na_2O	K_2O	P_2O_5	Total
KC14	178	62.01	1.21	17.15	4.25	0.12	1.35	3.01	5.97	3.59	0.38	99.03
		61.35	1.15	17.14	4.05	0.14	1.36	3.01	5.98	3.52	0.40	98.09
		60.59	1.26	17.03	5.06	0.13	1.82	3.59	5.62	3.22	0.60	98.93
		62.39	1.42	16.73	4.07	0.02	0.99	1.64	5.26	5.58	0.39	98.49
		63.79	1.00	17.25	3.84	0.34	1.28	2.64	5.42	3.88	0.41	99.85
	292.7	60.51	0.09	25.71	0.91	0.16	0.07	7.22	7.37	0.63	0.12	102.78
		65.68	1.20	16.40	3.70	0.04	1.06	2.25	6.24	3.88	0.62	101.08
		64.03	1.36	17.67	4.85	0.06	1.31	2.48	6.65	3.48	0.57	102.46
		62.13	1.23	17.17	5.07	0.14	1.70	3.35	4.57	3.43	0.51	99.30
		60.81	1.34	16.83	5.48	0.12	1.69	3.40	5.52	3.30	0.29	98.79
	776	59.36	0.95	15.61	7.62	0.25	2.85	4.28	2.73	5.15	0.72	99.54
		63.08	0.80	17.85	4.24	0.00	0.95	5.14	4.27	3.11	0.44	99.90

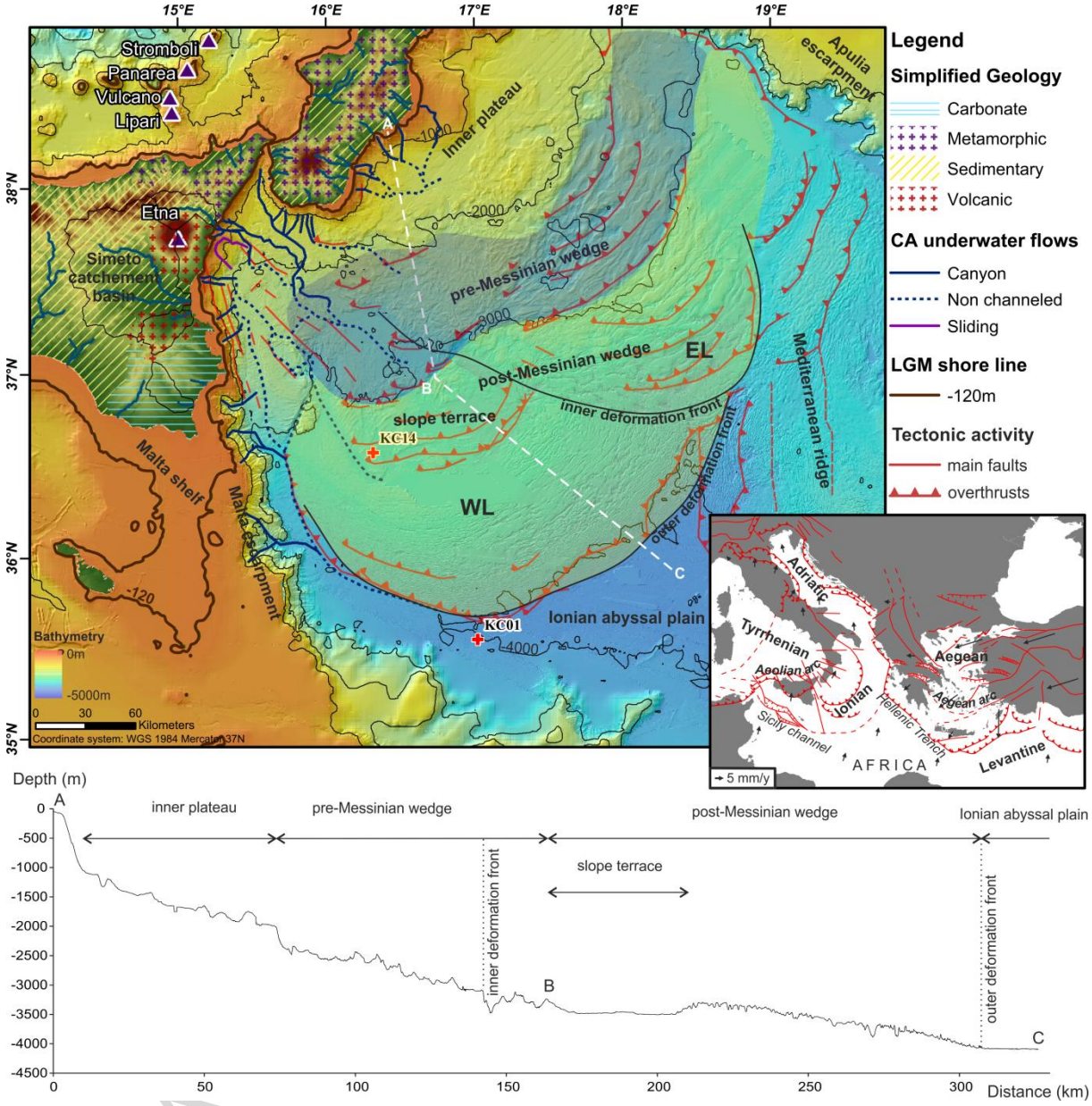

Fig. 1

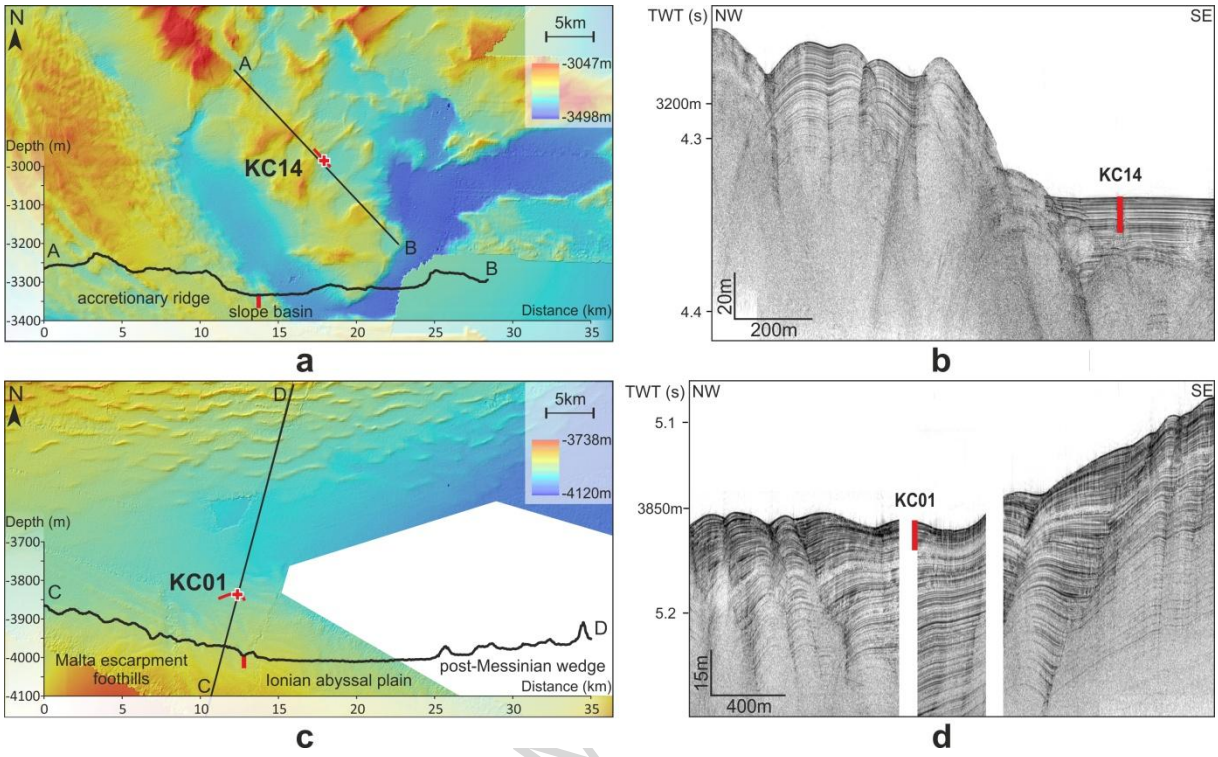

Fig. 2

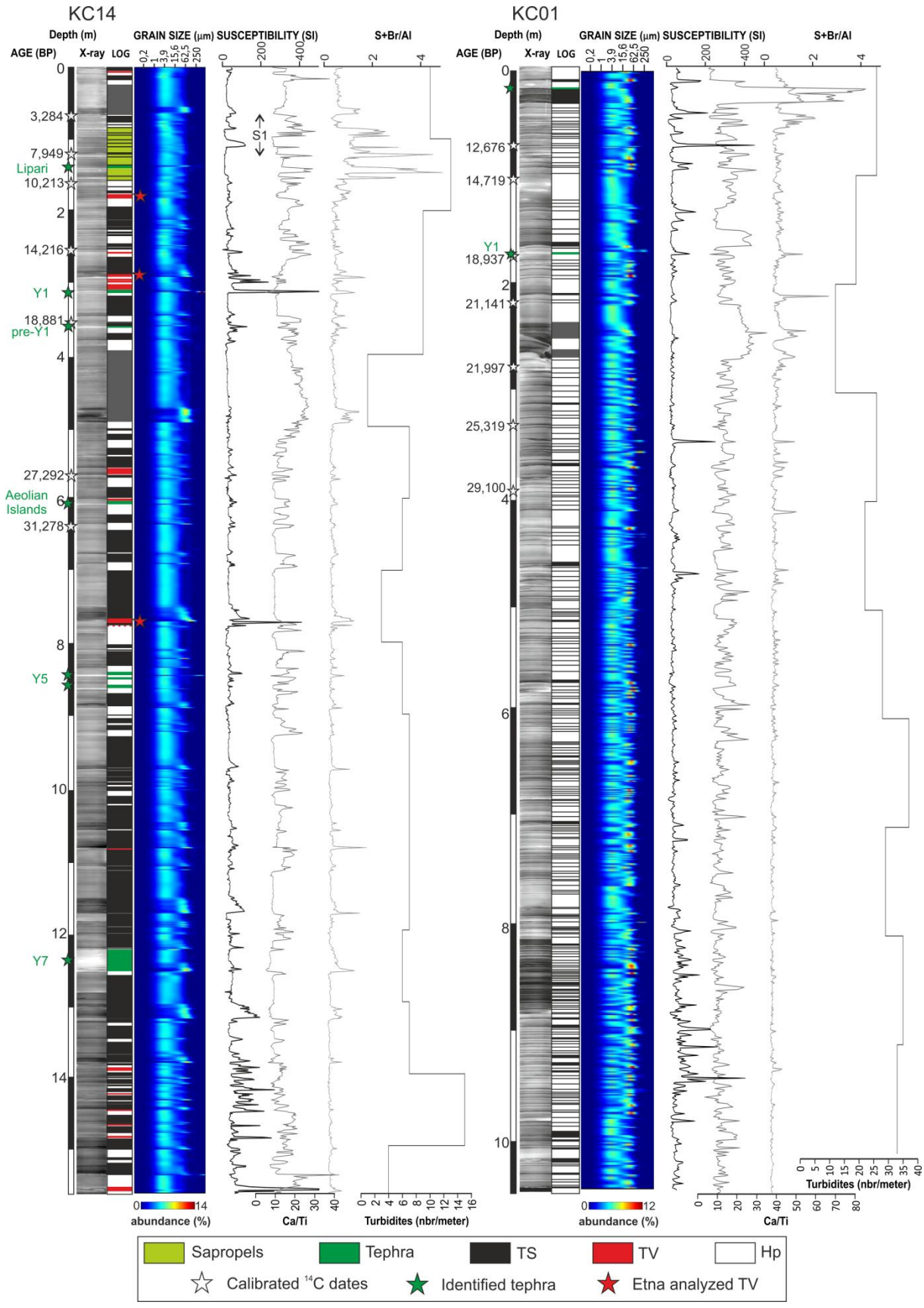
KC14
KC01
Depth (m)
AGE (BP)
X-ray
LOG
GRAIN SIZE (µm)
SUSCEPTIBILITY (SI)
S+Br/Al
S1
Lipari
Y1
pre-Y1
Aeolian Islands
Y5
Y7
abundance (%)
Ca/Ti
Turbidites (nbr/meter)
Sapropels
Tephra
TS
TV
Hp
Calibrated 14C dates
Identified tephra
Etna analyzed TV

Fig. 3

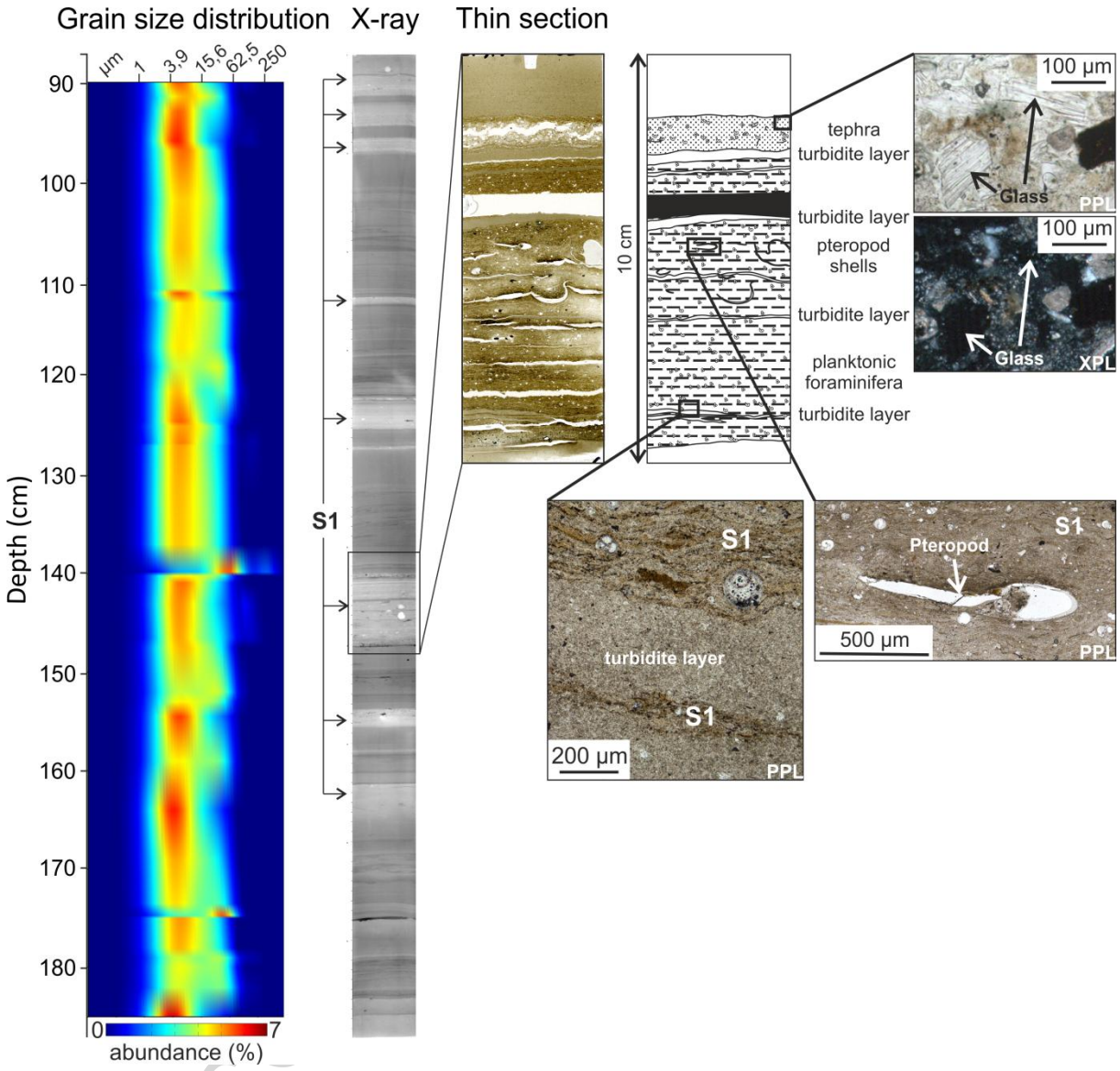

Fig. 4

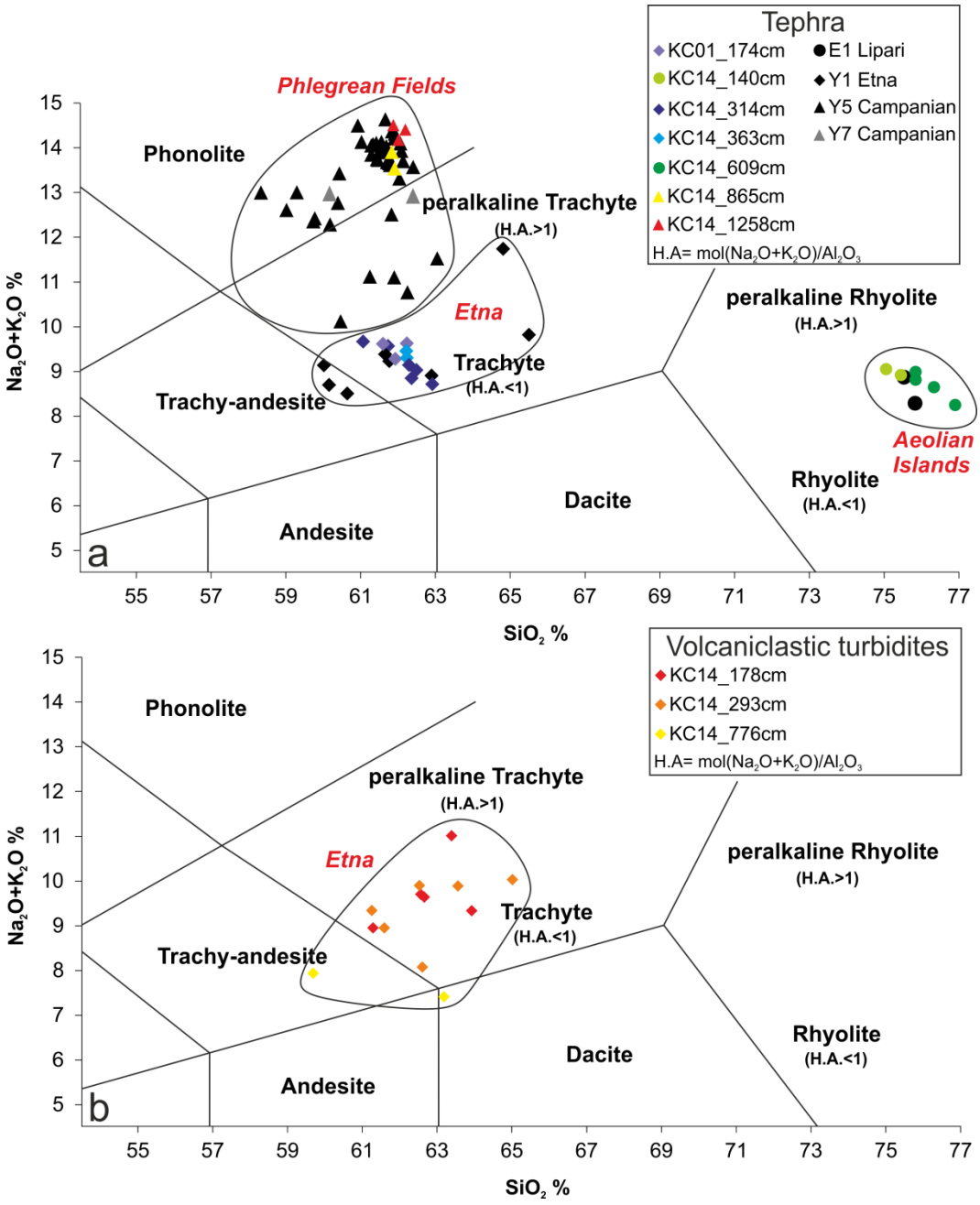

Fig. 5

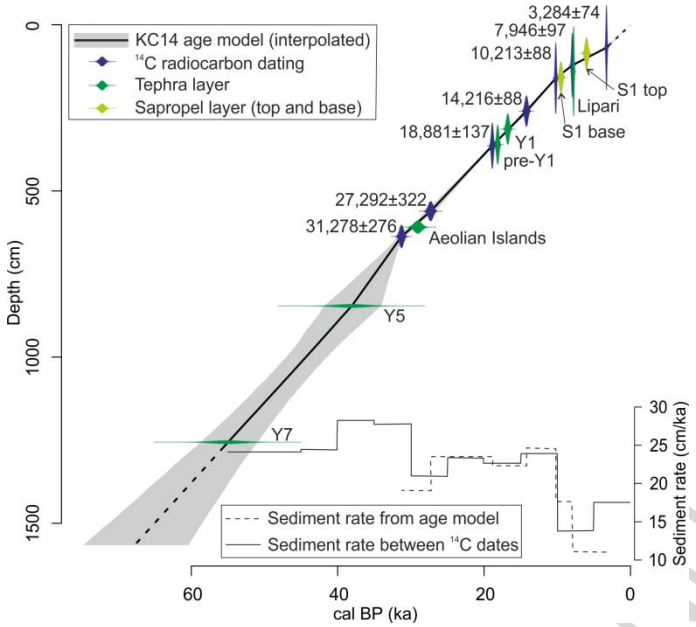

Fig. 6

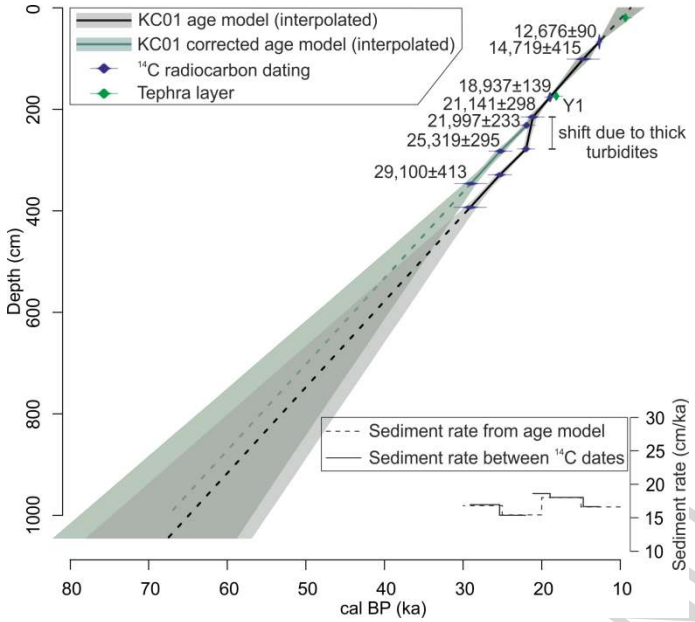

Fig. 7

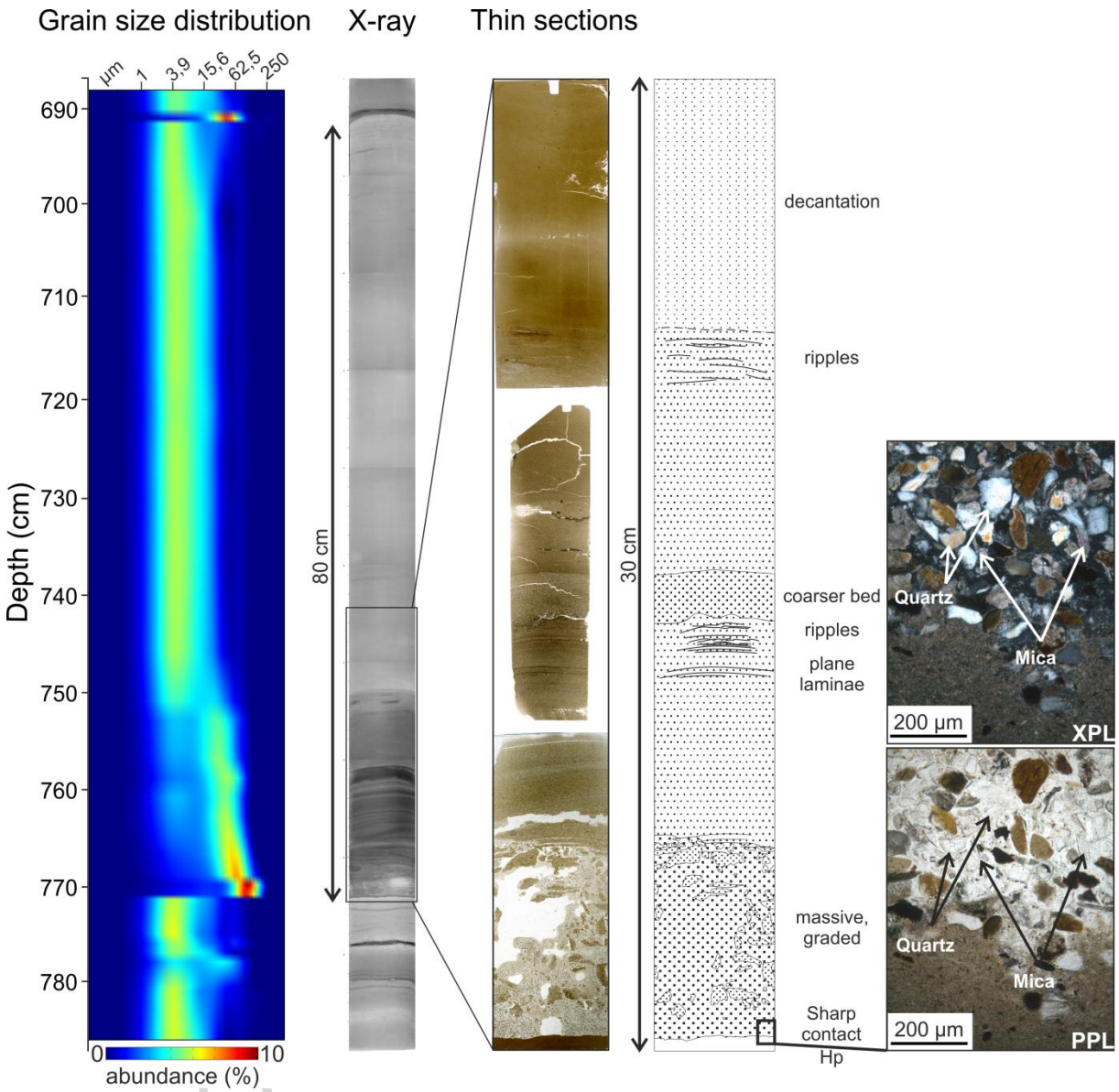

Fig. 8

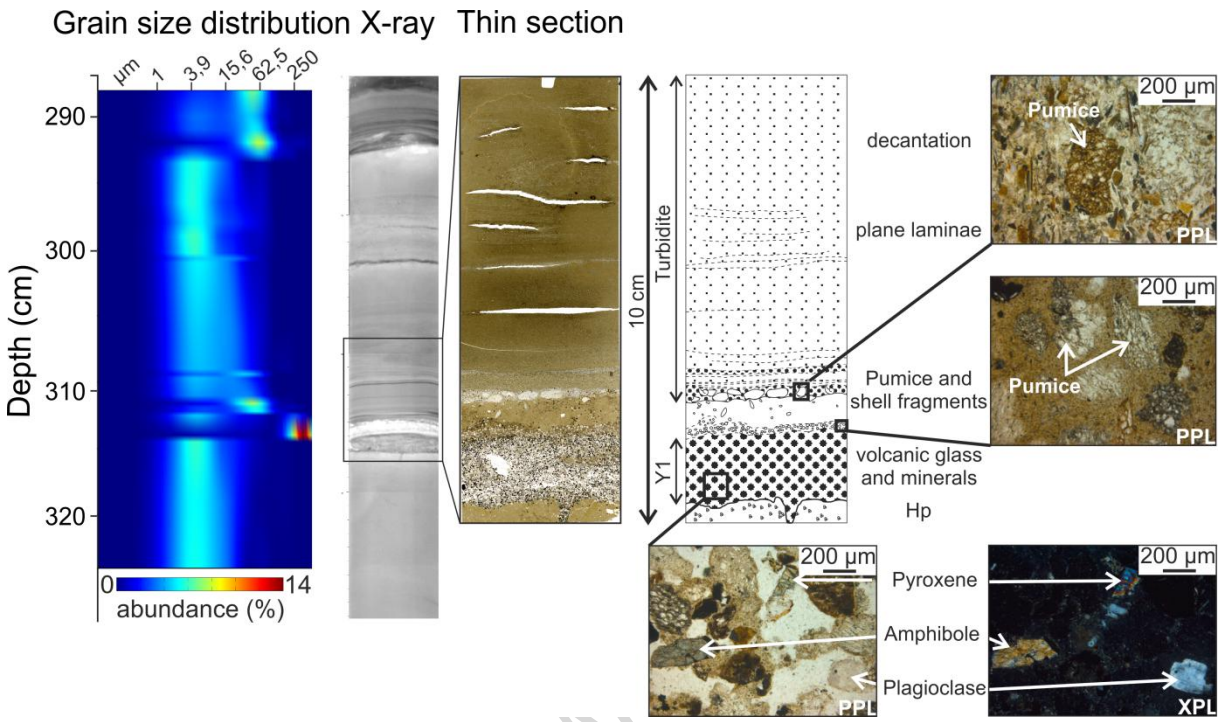

Fig. 9

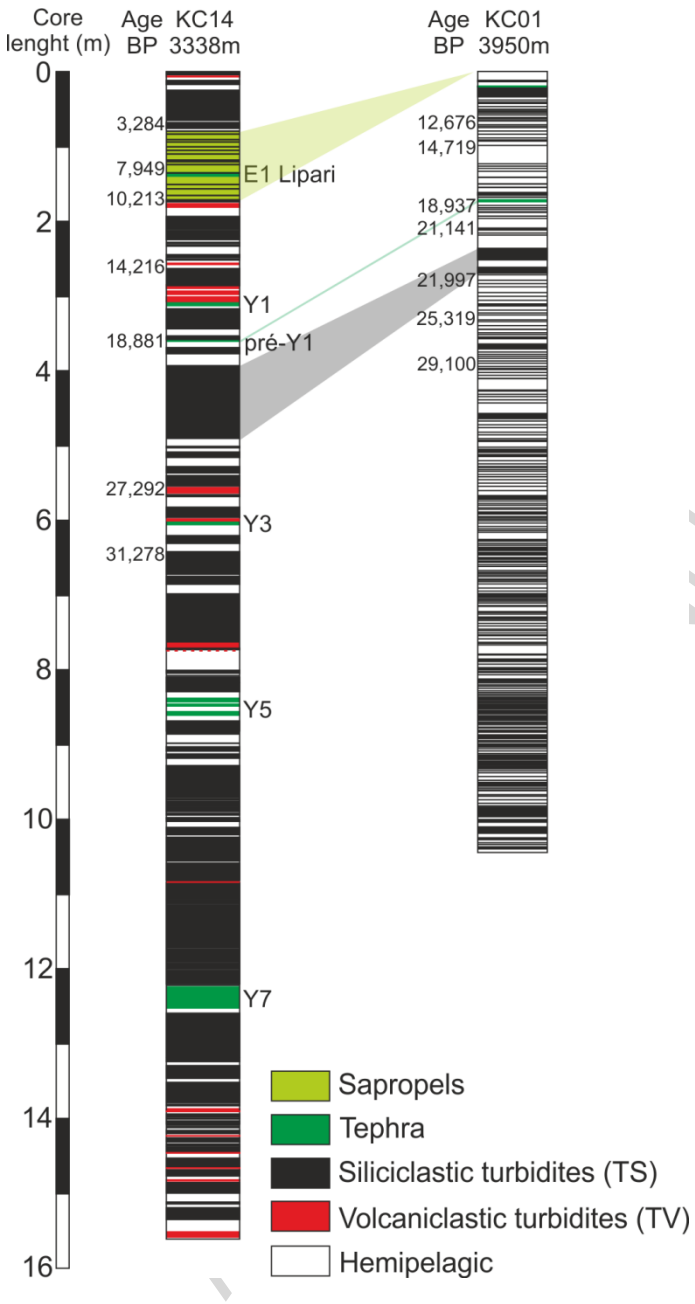

Fig. 10

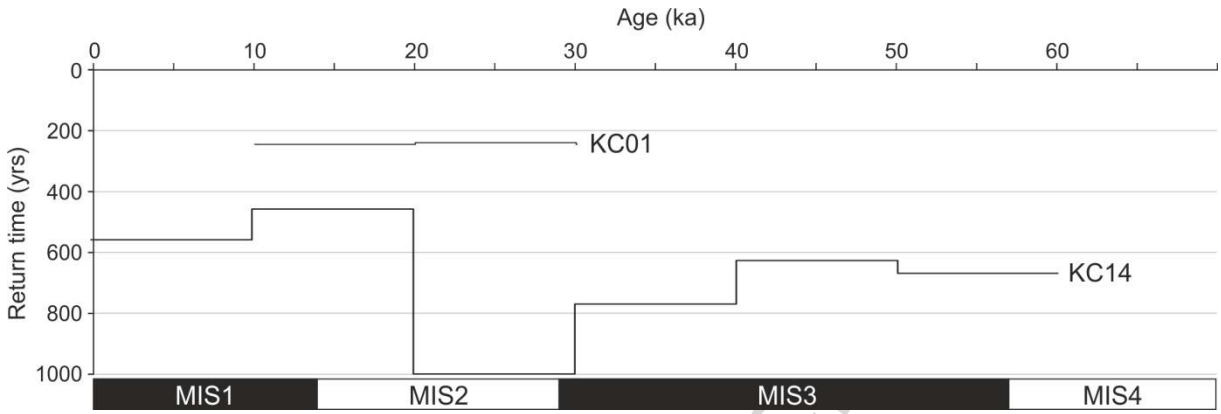

Fig. 11

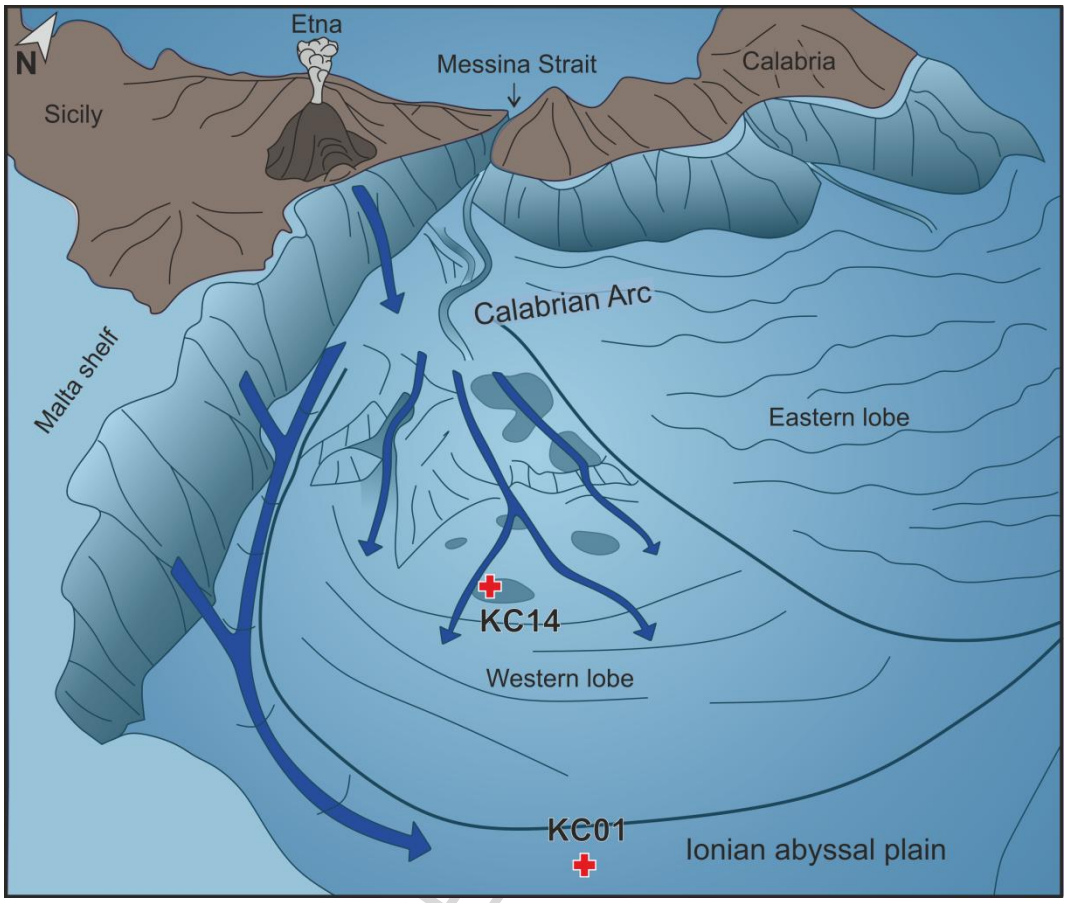

Fig. 12

Highlights

- Various origins and processes for turbidites are distinguished on the Calabrian Arc.
- A paleoearthquakes calendar has been defined on the last 60 ka.
- Co-seismic turbidites have a return time of 240 years in the abyssal plain and 450 to 1000 years in slope basins.
- A co-tsunami turbidite has been linked with the Cape-Riva Santorini caldeira collapse.
- Volcaniclastic turbidites are linked to Etna flank collapses.